CHAPTER 5 SLIDING BEARINGS: EXPERIMENTAL AND NUMERICAL ANALYSIS

5.1 Introduction

In the preceding chapter, the focus was on the application of HDRB and LRB in seismic isolation systems. However, this chapter examines an alternative seismic isolation approach involving a scaled moment-resisting frame structure with a sliding base integrated with conical and helical springs.

Due to the practical limitations of scaled-down HDRB and LRB units compatible with the scaled frame model within the limit of the available shake table, the sliding base mechanism with spring attachments was adopted. The sliding base system, supported by conical and helical springs, is intended to emulate the isolation properties of HDRB and LRB while being adaptable for small-scale experimental modeling. This setup allows the frame to exhibit controlled lateral displacements under dynamic loading conditions, providing insights into the behavior of base-isolated structures under simulated seismic loads.

Sliding bearing systems utilise displacement for passive energy dissipation and are based on the basic friction theory. Their primary benefit is their capacity to manage a wide variety of frequencies while limiting the maximum acceleration imparted to the superstructure by altering the friction coefficient [187]. Several studies have studied the use of sliding bearings for seismic isolation of structures and facilities [42][188][189]. A Friction Pendulum System is a sliding bearing that uses gravity as its restoring force, with an articulated friction slider on a spherical concave surface. The surface's continuous curvature maintains a stable friction coefficient, allowing for good seismic energy dissipation and structural protection [82]. The study was performed to control the seismic responses of a 10-story RC building

model, isolated by conventional sliding bearings, subjected to both near- and far-fault ground motions [187]. The parametric study was performed on liquid storage tank inserted with curved surface sliding bearings by Abali [190], nuclear power plants inserted with sliding bearing [191] and Reinforced-Cut-Wall [53]. The study looks at the selection of self-lubricating antifriction materials for pendulum sliding bearings used as seismic dampers in essential structures such offshore platforms in earthquake-prone locations. Computer models are used to analyse the thermal behaviour of these dampers, allowing for material selection depending on temperature resistance [192]. Nonlinear analyses are conducted on a 3D fiber model of both original and retrofitted structures. The CFRP behavior is idealized using an elastic linear model up to tension failure, while elastomeric bearings are modeled with a viscoelastic linear approach and sliding bearings with a bilinear model [118]. A prior study evaluated fixed base, sliding base, and sliding base with conical springs on steel frames. The proposed composite device, combining a flat sliding bearing with nonlinear stiffening springs, showed flat sliding behavior under moderate shaking, reduced peak displacements during intense shaking, and minimized residual displacements. Experiments on steel moment-resisting frames confirmed its effectiveness [83]. Further the design aids for nonlinear analysis of RC frame structure has been given in literature [193], [194].

This chapter presents an experimental study of sliding bearings in a scaled-model building construction. Given the potential benefits of steel building construction in seismic prone areas, a multi-floor steel frame was selected as the test model. The study emphasises on both the effectiveness of the isolation mechanism and the performance of the sliding bearing. The chapter is structured as follows: The "Experimental Setup" section discusses how to set up the shaking table for testing. The "Cases of Shaking Table Test" section looks at the dynamic

behaviour of the structural model with and without isolators (conical spring and circular spring). This system was tested at the Structural Dynamics Laboratory, Department of Civil Engineering, IIT BHU. This chapter discusses the testing procedure, observations, and performance of the sliding base system. The findings contribute to a comparative understanding of different isolation technique in enhancing the resilience of moment-resisting frame structures against seismic events.

5.2 Methodology

The methodology for this investigation involved fabricating a scaled three-story, single-bay moment-resisting frame using steel square bars for the beams and columns. Each section was cut to the required dimensions with a precision cutting machine to ensure consistent structural properties. For the sliding base configuration, additional steel plates were prepared to act as bottom and top sliders. The bottom slider plates were secured to the shaking platform within angle sections, providing a stable base. The top slider plates were attached rigidly to the columns of the frame structure to enable movement when the base shear surpassed the friction threshold. Springs were then attached at 100 mm from the frame's base, offering controlled resistance and simulating realistic dynamic behavior as shown in Figure 5.1. This precise arrangement allowed the frame to exhibit sliding and damping characteristics necessary for analyzing base isolation effects under simulated seismic conditions. Each aspect of the setup ensured reliable testing outcomes, facilitating a comprehensive evaluation of base isolation performance.

(a) (b)

Figure 5.1 A three-story moment-resisting frame structure was installed in a test chamber at the Structural Dynamics Laboratory, Civil Engineering Department, IIT-BHU, Varanasi. (a) shows the frame structure with applied loads and a sliding base connected to springs, while (b) shows the frame structure with a fixed base without applied load.

To perform the sliding base analysis with and without the spring combination, ground motions with varying Peak Ground Accelerations (PGAs) were selected. These ground motions, spanning a range of PGAs, were applied as input to a shaking table machine in the Dynamics Laboratory of the Civil Engineering Department at IIT-BHU, Varanasi. The frequency corresponding to the maximum PGA was determined using SeismoSignal software, ensuring accurate simulation conditions. Using frequency-based input derived from the peak Fourier amplitude is a suitable approach for one-dimensional shake table testing. By identifying the dominant frequency of ground motion with SeismoSignal, the input reflects the primary shaking frequency, capturing the main seismic impact relevant to the structure's response. This approach simplifies testing while targeting the most critical frequency for structural behavior

in the tested direction, aligning with standard seismic testing practices to effectively replicate the primary characteristics of real seismic events.

The shaking table's amplitude was set at fixed values of 25 mm and 45 mm to examine the structural response under these conditions. The amplitude is within the operational limits of the shaking table in the IIT-BHU laboratory. The analysis revealed that at higher amplitudes, the structural responses increased significantly, indicating a notable sensitivity of the structure to amplitude variations. The results were also compared with those from a fixed base, providing insights into the effects of sliding base behavior on structural response under dynamic loading.

5.2.1 Experimental Arrangement

The shaking table test utilized a quarter-scaled of length of a three-story, single-bay moment-resisting steel frame structure, inspired by an office building in California, USA [195]. This prototype structure was tested to evaluate the effectiveness of various sliding bearings in a controlled laboratory setting. The models first story has a height of 0.5 meters, while the second and third stories are 0.4 meters each. Both the columns and beams of the structure are solid, homogeneous square steel sections, providing uniform material properties and structural consistency. The beam lengths are 716 mm and 800 mm, and both beams and columns have cross-sectional dimensions of 12 mm × 12 mm. The tensile strength test showed a yield strength of 470 MPa and an ultimate load of 803.8 MPa for the bar as shown in Figure 5.2.

Figure 5.2 UTM set up to measure the tensile strength of a 12 mm bar at Structural Engineering Laboratory, Civil Engineering Department, IIT-BHU, Varanasi

To simulate realistic mass distribution, a mass of 18 kg was attached at the top story, with additional masses of 22.3 kg each affixed to the second and first stories. These masses, configured as solid circular rods, are rigidly connected to the frame at equal distribution of loads, ensuring they do not affect the structure's inherent stiffness along the shaking direction. The rigid attachment of these masses allows the frame to respond realistically to lateral forces, closely mimicking the dynamic behavior of an actual building. This setup effectively replicates the intended seismic response, allowing for comprehensive analysis of base isolation through sliding bearing performance.

5.2.2 Sliding Base Setup

The experimental setup for the sliding base considered four large steel plates (385mm × 285mm) serve as the bottom plate, which is securely attached to the shaking platform. Four smaller steel plates (80mm × 80mm) are rigidly connected to the bottoms of the frame columns and act as the top sliders. In this setup, the smaller plates with the frame are placed on the larger bottom plates. When the base shear in the model frame exceeds the frictional threshold between the top and bottom sliders, the top sliders initiate sliding over the bottom plates. This sliding mechanism simulates a base isolation effect, where movement occurs only if the applied shear force surpasses the static friction limit, allowing the structure to exhibit controlled displacement during dynamic loading. This setup effectively demonstrates the base isolation concept under experimental conditions. The schematic Figure 5.3 shows the base sliding base isolation setup on shaking table platform.

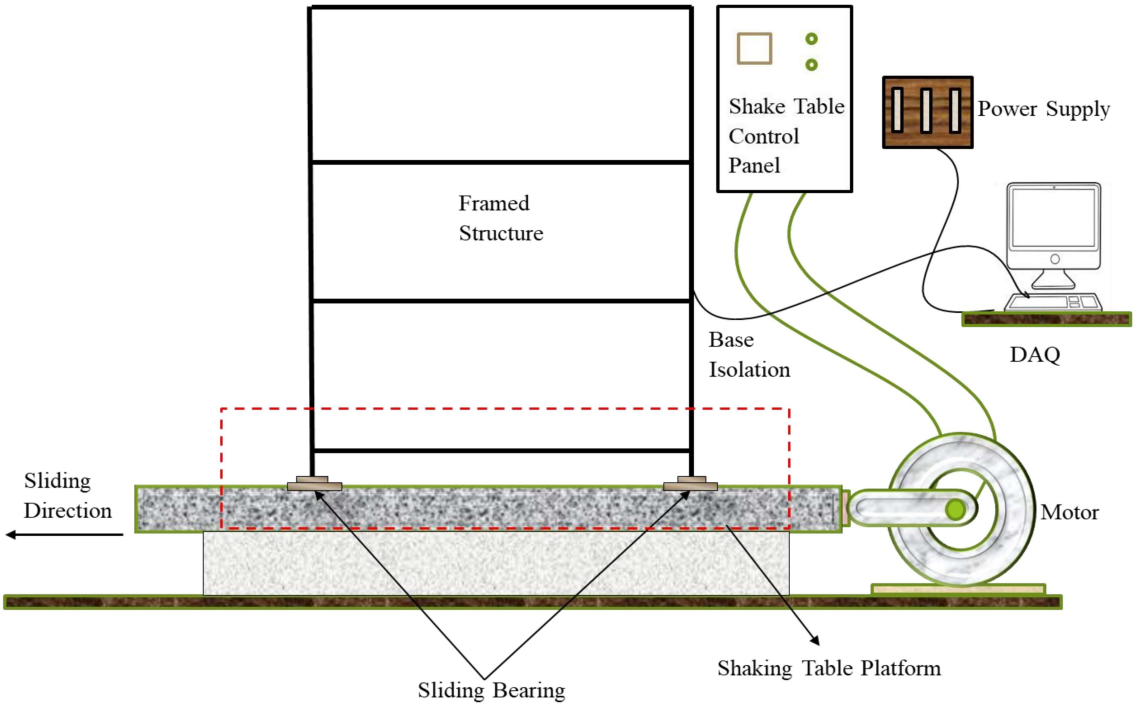

Figure 5.3 Schematic representation of the shaking table setup with a frame structure equipped with sliding bearings

5.2.3 Sliding Base with spring

The spring design must ensure it fits between the bottom slider and column, with an adjustable pitch to accommodate a full range of force-deformation behaviors, from low-stiffness linear responses in mild motions to high-stiffness nonlinear responses in strong motions. A carefully chosen wire diameter provides low initial stiffness for smooth motion, while the diameter ratio of larger to smaller loops enhances the spring's hardening effect. The loop counts and spacing should be minimal yet uniform, with adequate loop size to allow for local fabrication without compromising mechanical performance.

5.3 Determining the Coefficient of Friction

To determine the static friction coefficient between the steel plates of the top and bottom sliders, the structure, with the top slider as its base, was loosely positioned on the shake table, resting on the bottom slider. A string was attached to the bottom frame, allowing horizontal force to be applied to the structure using a pulley system, as illustrated in Figure 5.4. The load on the pan was gradually increased from zero until the base began to slide. The table provides the experimentally determined static friction coefficient values. In the table, F represents the minimum load necessary to initiate sliding, W indicates the structure's weight, and μs signifies the static friction coefficient. The experiment resulted in an average static friction coefficient of 0.23, with trials demonstrating consistent repeatability.

Figure 5.4 String-Pulley laboratory test setup for the calculation of the friction value in a test chamber at the Structural Dynamics Laboratory, Civil Engineering Department, IIT-BHU, Varanasi.

5.4 Shake Table Setup

Structural response data from real earthquakes can be unreliable due to uncontrolled factors like soil conditions, unknown input motions, and pre-existing structural damage. Observations, though valuable, often lack systematic documentation. Shake tables provide the most reliable method for studying earthquake effects on structures. Designed specifically for this purpose, they help identify causes of damage or reasons for resilience in structures. While modern six-dimensional shake tables offer precise earthquake simulations, they are complex and costly to operate and maintain. The shake table used in the experiment was a servo-hydraulic operated uniaxial shake table properties presented in Table 5.1. For the experimental study, a high-performance Type 3050-A-060 based 6-channel Input Module LAN XI 51.2kHz data acquisition system from Bruel and Kjaer National Instruments, USA was used and Bruel & Kjaer PULSE LabShop Version 18.1.0.28 program was used to view and record the output of various sensors. Five accelerometers were used to measure the accelerations and

displacement at different points: one on each of the three floors, one above the base of the structure, and one on the shake table. All sensors were positioned with their axes aligned to match the direction of the input motion, as illustrated in Figure 5.5.

Table 5.1 Characteristics of Horizontal Shake Table at IIT, Varanasi

Motion	Horizontal (Unidirectional)
Shake Table Size	1500 mm × 1200 mm
Frequency Range	0-20Hz
Maximum Pay Load	200 Kgs
Maximum Height of Model	1500 mm
Tentative ‘g’ value	0.1g-3g
Amplitude	+/- 50 mm or Total 100 mm

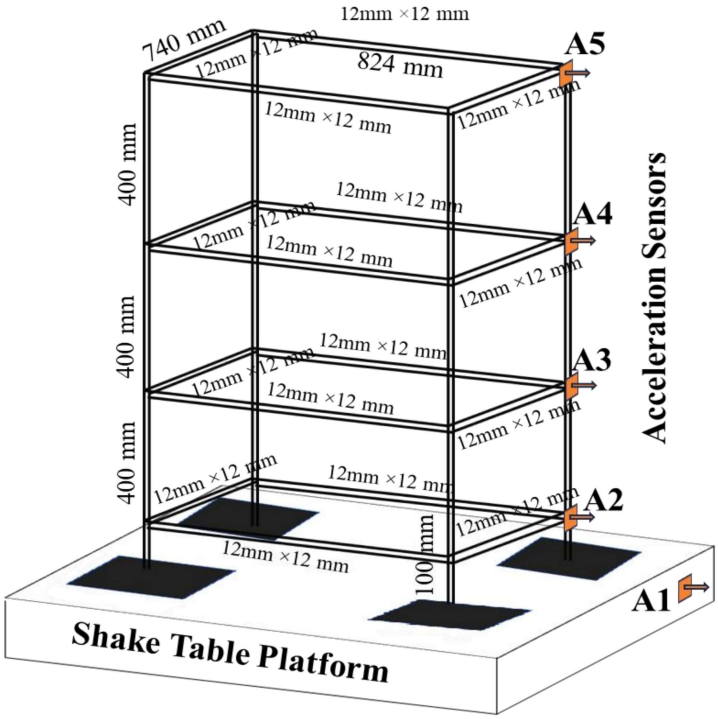

Figure 5.5 Schematic representation of the sensor locations in the moment resisting frame structures model on shake table platform

5.5 Dynamic Characterization of the model using Pulse Labshop Software

The Bruel & Kjaer (B&K) 4507 accelerometer is a high-precision device ideal for vibration measurement applications, including shake table testing of moment-resisting frame structures as shown in Figure 5.6. It features a robust design, wide frequency range, and high sensitivity, making it suitable for dynamic analysis of these structural systems. Compatible with Pulse LabShop software for data acquisition (DAQ), it enables real-time signal processing, analysis, and visualization of vibration data. This seamless integration allows efficient monitoring and analysis of acceleration and dynamic responses, providing accurate insights into the behavior of moment-resisting frames during shake table experiments.

The B&K 4507 accelerometer was used to measure the vibration motion of the moment-resisting frame structure. Before starting the measurement process, the accelerometer's measuring range was set based on the expected acceleration values to ensure accurate data collection. This setup allowed for reliable monitoring of the structure's dynamic response, capturing vibrations effectively within the defined range.

Figure 5.6 Accelerometer Bruel & Kjaer Type 4507 in Structural Dynamics Laboratory, Civil Engineering Department, IIT-BHU, Varanasi.

5.6 Impact Hammer

The impact and vibration response signals were acquired using a Bruel & Kjaer Type 3050-A-060 6-channel Input Module LAN XI, operating at 51.2 kHz data acquisition rate. The experimental setup utilized PULSE LabShop Fast Track Version 18.1.0.28 software to obtain the Frequency Response Functions (FRF), with the impact hammer type Bruel and Kjaer 8206-003 (shown in Figure 5.7) is used for excitation and accelerometer type Bruel and Kjaer 4507 is used for response. To prevent aliasing, the acquisition rate was set to approximately three times the bandwidth excited by the hammer. Exponential windows were applied to both the force pulse and vibration response signals to mitigate leakage effects. FRFs were calculated by averaging five individual measurements to ensure accuracy and consistency in the data.

The data collected from the measuring station, including both excitation and response signals, were transformed from the time domain to the frequency domain using the Fast Fourier Transform (FFT) within the PULSE LabShop software. The resulting Frequency Response Functions (FRFs), which represent the ratio of response to excitation force in the frequency

Figure 5.7 Impact hammer type Bruel and Kjaer 8206-003 in Structural Dynamics Laboratory, Civil Engineering Department, IIT-BHU, Varanasi.

domain, were then analyzed to identify the fundamental natural frequencies of the system as shown in Figure 5.8. Once the data were processed, the results were transferred to a PC for post-processing using Excel, where modal parameter extraction was performed, allowing further insights into the dynamic characteristics of the system under study.

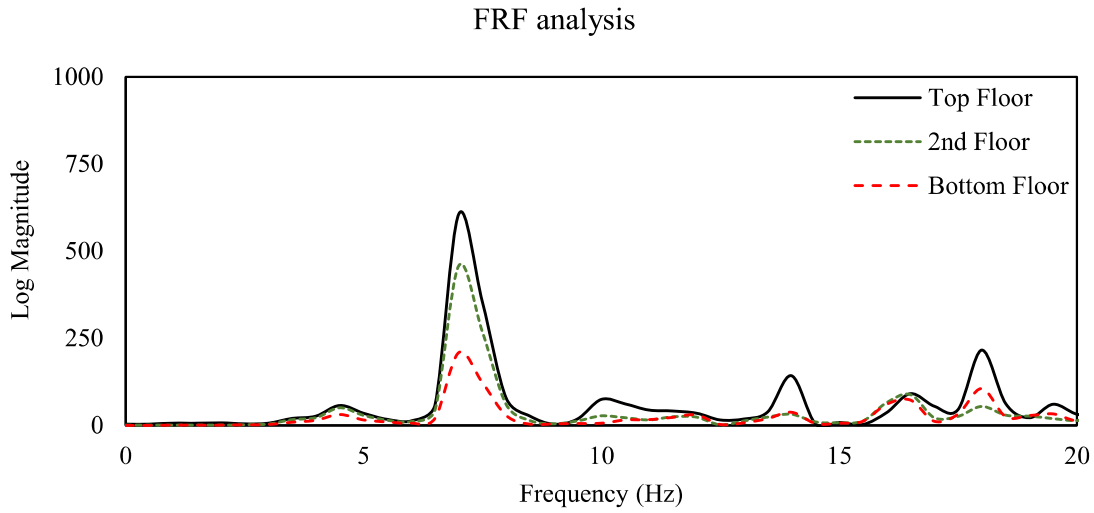

Figure 5.8 The frequency response function for three story moment resisting frame structure.

5.7 Spring Compression Testing

The linear and non-linear spring were tested using Tinius Olsen UTM 10KN as shown in Figure 5.9. The rate to loading is 10mm/min is applied on the spring. The HORIZON software package is used to identify the compression response of the both springs. An experiment was conducted to determine the force-deformation behavior of a conical spring and a linear helical spring under compression. The experimental setup, as shown in Figure 5.9, illustrates the process for obtaining the force-deformation curve of the spring. In this setup, one end of the spring was fixed, while the other end was attached to a lightweight square plate. This movable end was gradually compressed towards the fixed end until most of the spring loops made contact. The resisting force generated by the spring during compression was measured using

a load cell, while the deformation was recorded by a UTM compatible with the HORIZON software package.

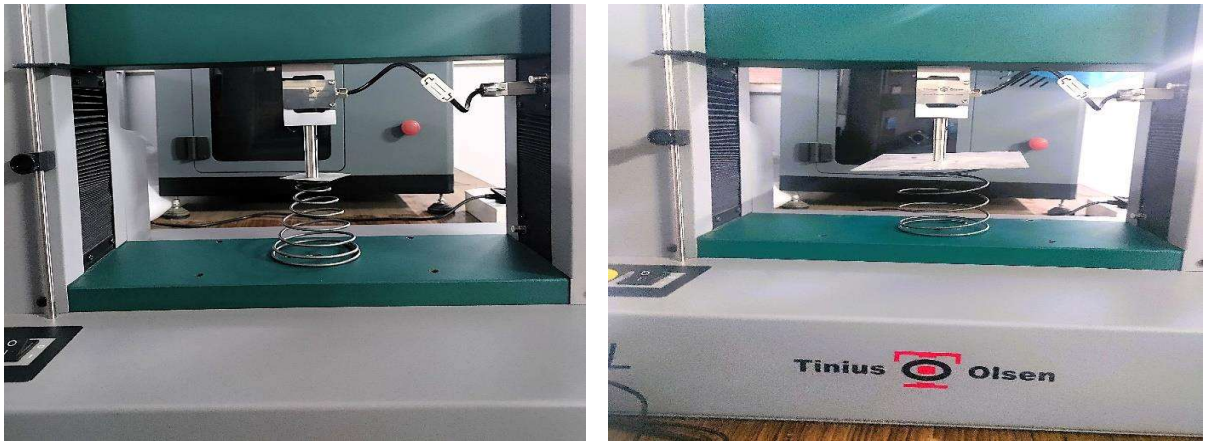

(a) (b)

(c)

Figure 5.9 The UTM test setup for (a) Non-Linear Spring (b) Low Stiffness Linear Spring and (c) High stiffness Linear Spring at IIT-BHU laboratory

5.7.1 Dimension of the Springs

The dimensions of the conical spring with larger diameter 85 mm, smaller diameter 25mm, number of loops 6, wire thickness 3.25 mm and value of pitch is 16 mm, low stiffness linear spring having diameter 85 mm, number of loops 5, wire thickness 3.25 mm and pitch 22 mm and high stiffness linear spring having diameter 49 mm, number of loops 4, wire thickness 2.75 mm and pitch was taken as 22.5 mm. The spring length is chosen to fit within the

available space, with a pitch that supports both linear and nonlinear behavior. The wire diameter should provide appropriate initial stiffness, while its dimensions ensure adequate stiffness variation. A well-balanced number of loops with uniform pitch and suitable loop size is essential for efficient fabrication and installation.

5.7.1.1 Conical Spring

Conical springs, or non-linear springs, achieve the desired restoring behavior through progressive stiffness. The larger loops, being more flexible, were ground first, followed by smaller loops, increasing stiffness. This results in a multi-linear, hardening force-deformation response, making them suitable for base isolation systems. The conical spring is tested for force deformation using UTM machine compatible with Horizon software. The Figure 5.10 shows the force-deformation curve for the spring. The initial stiffness value 1.19 $\boldsymbol{N/mm}$ and the last stage stiffness value is 8.4 $\boldsymbol{N/mm}$.

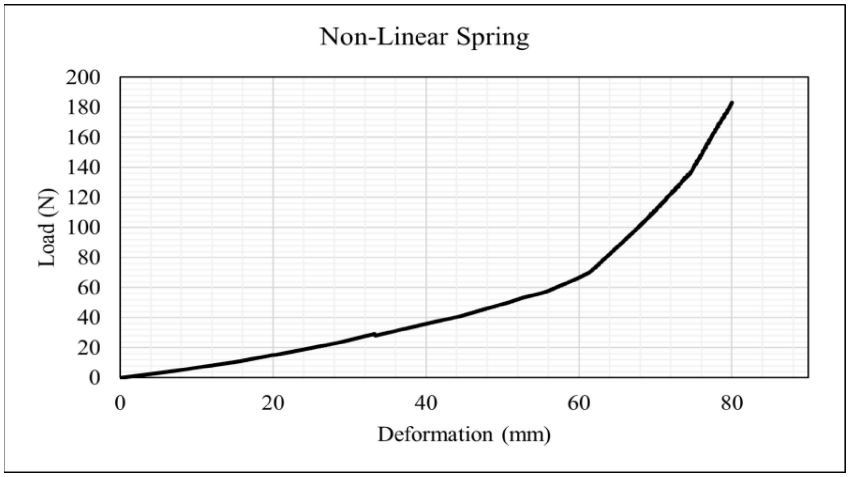

Figure 5.10 The force-deformation curve for the conical spring

5.7.1.2 Low Stiffness Linear Spring

The experimental results of the force-displacement curve for the linear spring were verified through numerical analysis using SOLIDWORKS 2023. The Figure 5.11 shows that the results align closely with the experimental data. The stiffness value is 0.31 N/mm. The Figure 5.12 shows the diagram for deformation of the spring.

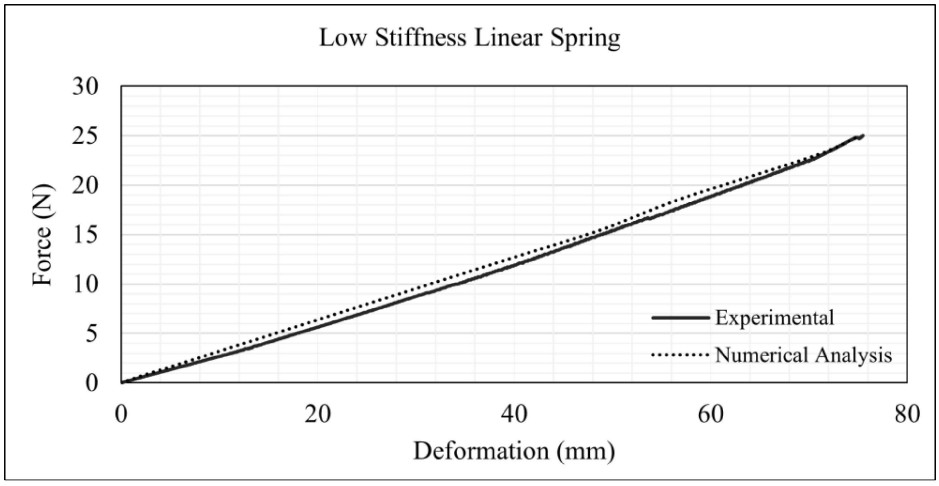

Figure 5.11 The force-deformation curve for the low stiffness linear spring

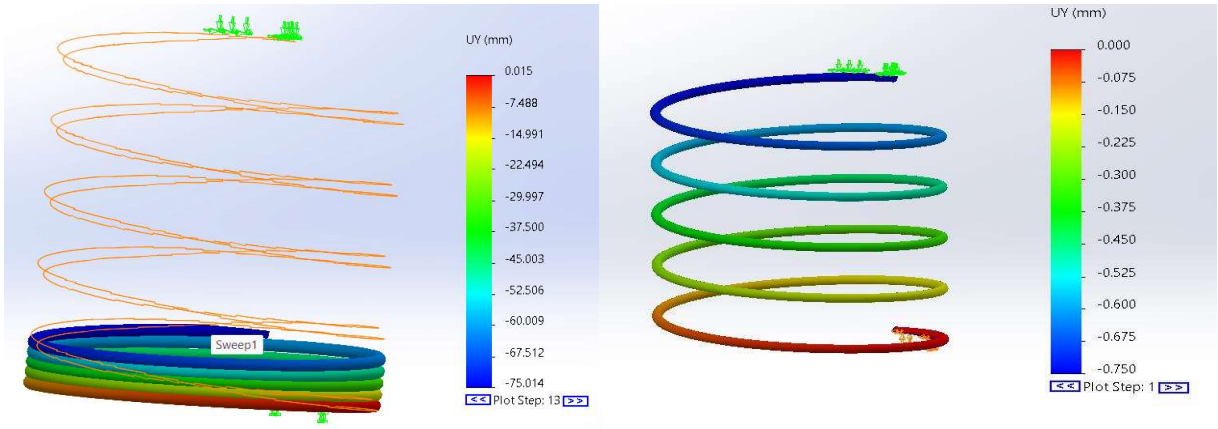

Figure 5.12 The low stiffness spring deformation obtained from numerical analysis of a using SOLIDWORKS software.

5.7.1.3 High Stiffness Linear Spring

The experimental results of the force-displacement curve for the linear spring were verified through numerical analysis using SOLIDWORKS. The Figure 5.13 shows that the results align closely with the experimental data. The spring stiffness value is 1.18 N/mm. The Figure 5.14 the diagram for deformation of the spring.

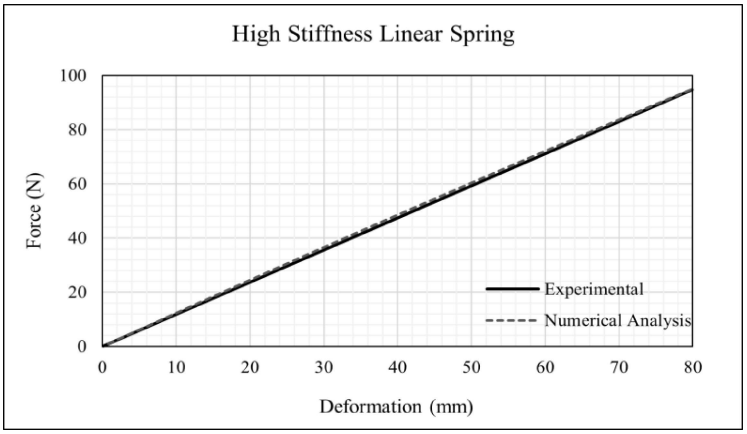

Figure 5.13 The force-deformation curve for the high stiffness linear spring

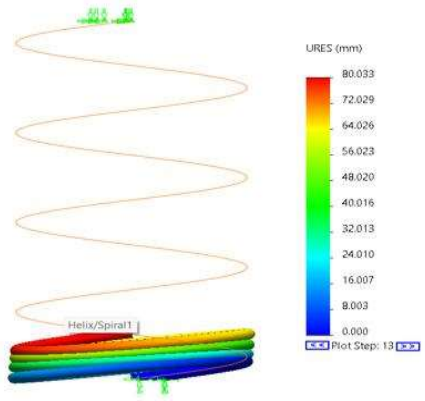

Figure 5.14 The high stiffness spring deformation obtained from numerical analysis of a using SOLIDWORKS software.

5.8 Properties of Earthquake Input Records

Seismic motion arises from sudden energy release during fault rupture, influenced by source mechanics, wave travel, and soil conditions. Earthquakes differ in magnitude, origin, distance, direction, and site effects. Choosing suitable acceleration records for nonlinear analysis is vital, as they impact structural response. The seismic records used in this study were selected from the Pacific Earthquake Engineering Research Center (PEER) database [176] for the Imperial Valley, Loma Prieta, Northridge, Kobe, and Chi-Chi earthquakes.

The frequency corresponding to the maximum PGA was determined using SeismoSignal software, ensuring accurate simulation conditions. Using frequency-based input derived from the peak Fourier amplitude is a suitable approach for one-dimensional shake table testing. The input ground motion and corresponding frequencies are shown in Table 5.2.

Table 5.2 Applied ground motion frequency for the present analysis

Event	Station	Year	Magnitude	Frequency (Hz)
Kobe	FUK	1995	6.9	0.79
ChiChi	TCU054	1999	7.62	0.98

Northridge	Pacoima Kagel Canyon	1994	6.69	1.24
Imperial valley	Meloland Geot. Array	1989	6.53	1.29
Kobe	Nishi-Akashi	1995	6.9	1.36
Loma Prieta	Capitola	1989	6.93	1.63

5.9 Numerical Simulation in Abaqus

This section discusses the numerical simulation of a fixed-base moment-resisting steel frame structure and a steel frame with a sliding base, analyzed both with and without springs. Subsequent sections provide a detailed explanation of the Abaqus procedures for both the fixed-base and sliding-base configurations. The Table 5.3 shows the first three mode value obtained from Abaqus numerical simulation. The mode shapes of the fixed base frame structure from Mode 1 to Mode 3 are shown in Figure 5.15.

Table 5.3 The first three mode shapes of the fixed-base frame structure.

Mode Number	Time Period (s)
Mode 1	0.30120
Mode 2	0.26810
Mode 3	0.17452

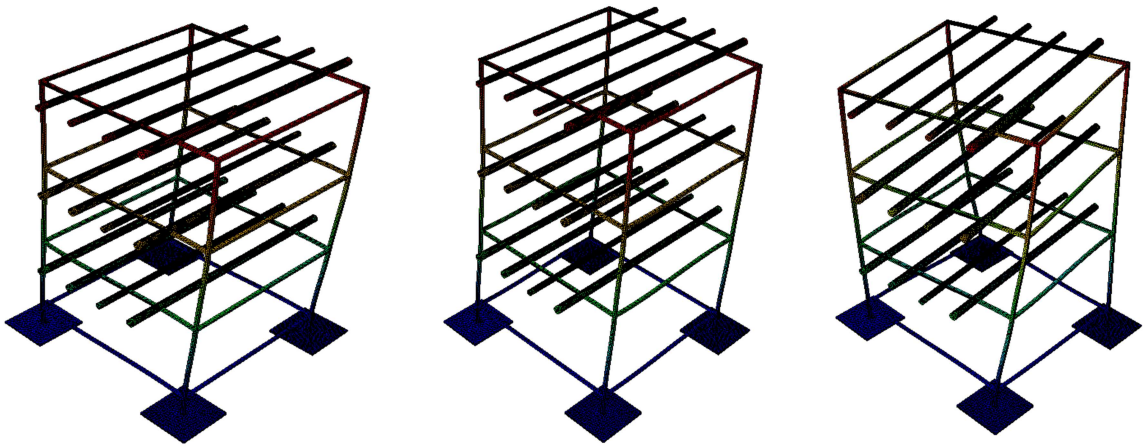

(a) (b) (c)

Figure 5.15 The diagram illustrates the mode shapes of the fixed-base structure corresponding to the first three modes, respectively.

5.9.1 Fixed Base Analysis

In this analysis, Abaqus was used to validate the experimental results through dynamic implicit analysis, focusing on simulating the behavior of a frame structure. The process began in the *Part Module*, where the frame geometry, comprising beams and columns, was constructed as a wireframe model. This approach allowed for a simplified yet effective representation of the frame's structural elements.

Material properties were assigned within the *Material Module*, where the density, modulus of elasticity, and Poisson's ratio were specified to accurately reflect the frame's behavior. The density was critical for the dynamic analysis, while the modulus of elasticity and Poisson's ratio ensured that the material responded realistically under loading. In the *Section Module*, a rectangular solid homogeneous bar section was defined with precise thickness, and this profile was subsequently assigned to the frame's beams and columns using the *Assign Section Module*. The *Step Module* facilitated the setup of analysis parameters, including the total analysis time, which was set to 4 seconds, and the increment size, which was carefully chosen to balance accuracy and computational efficiency. In the *Mesh Module*, the frame was discretized using B31 elements, a 2-node linear beam type, to ensure accurate representation of structural behavior in the dynamic analysis.

Load application was managed by defining the structural weight as a line load applied directly to the frame. To replicate the experimental conditions, the *Amplitude Module* allowed the input of displacement and acceleration values based on shake table data, directly imposing the experimentally derived amplitudes onto the model. Boundary conditions were applied to reflect the constraints of a one-dimensional shaking table test. Movement was allowed solely along the x-direction, with all other translational and rotational degrees of freedom restrained.

This setup accurately mirrored the uniaxial conditions of the experimental test, enabling a direct comparison between the simulation and experimental results. For output, the *Output Module* was used to select and configure the response parameters for analysis, ensuring that all relevant data points would be captured for subsequent evaluation. The Abaqus diagrams illustrating the steel frame structure under conditions with and without applied loads are presented in the Figure 5.16.

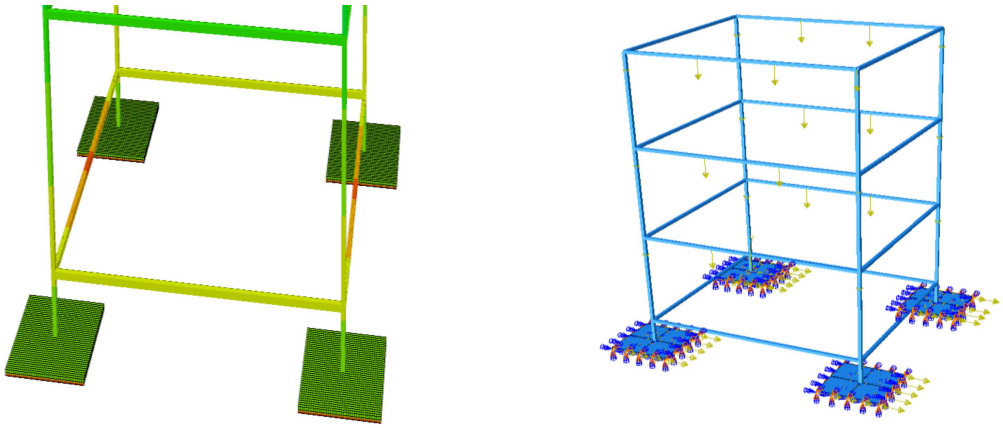

(a) (b)

Figure 5.16 The steel frame structure representation in two configurations: (a) A moment-resisting steel frame structure without any applied load (b) A steel frame structure subjected to applied load and boundary conditions

5.9.2 Sliding Base Analysis

In the sliding bearing case, Abaqus was employed to model sliding base experimental results via dynamic implicit analysis to simulate the behavior of a frame structure and plates. Geometry was created in the *Part Module*, modeling the frame as a wireframe of beams and columns, and the plates as solid homogeneous sections for accurate structural representation. Material properties—density, modulus of elasticity, and Poisson's ratio—were defined in the *Material Module* to ensure realistic response under dynamic loads, while the *Section Module*

assigned a rectangular solid section to the frame and a solid homogeneous section to the plates. Analysis parameters, including a 4-second duration and optimized increment size, were set up in the *Step Module*, with response outputs configured in the *Output Module*.

The *Interaction Module* was central to defining key interactions. An MPC interaction connected the top plates and frame, while sliding friction was applied as a penalty in the tangential behavior settings. Hard contact was enforced between the plate surfaces through normal behavior specifications. Meshing was handled in the *Mesh Module*, using B31, 2-node linear beam elements for the frame and C3D8R, an 8-node linear brick, reduced integration, hourglass control, hex elements for the plates. Line loads represented structural weight, while shake table amplitudes were applied in the *Amplitude Module* as displacement and acceleration. Boundary conditions restricted movement to the x-direction only, mirroring the one-dimensional shake table constraints for direct comparison with experimental data. The Numerical simulation in Abaqus for sliding base and sliding base with loading condition are shown in Figure 5.17.

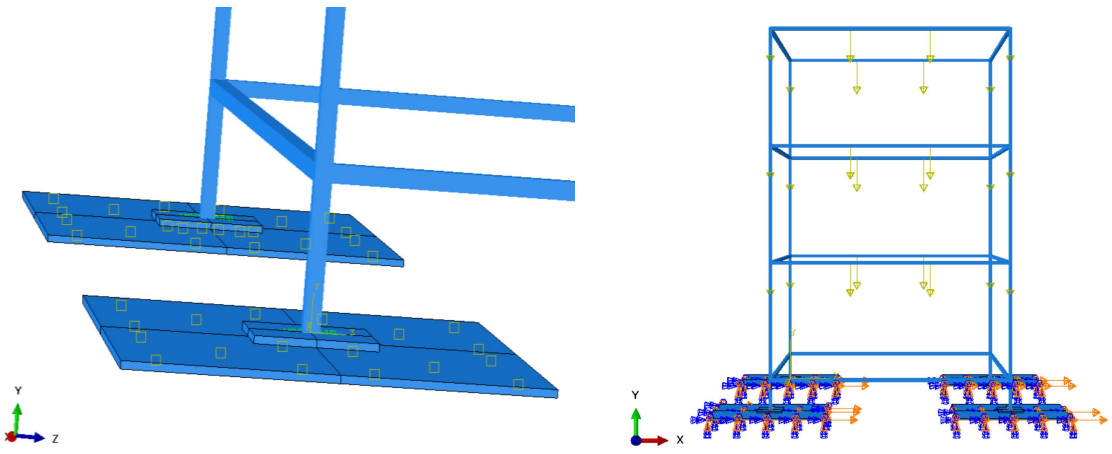

(a) (b)

Figure 5.17 The diagram (a) shows the interaction between the plates in Abaqus and (b) shows the loading condition in sliding base case

5.10 Comparison of Results

This study involves five types of analyses: fixed base, sliding base, sliding base with a low-stiffness linear spring, sliding base with a high-stiffness linear spring, and sliding base with a nonlinear spring as shown in Figure 5.18.

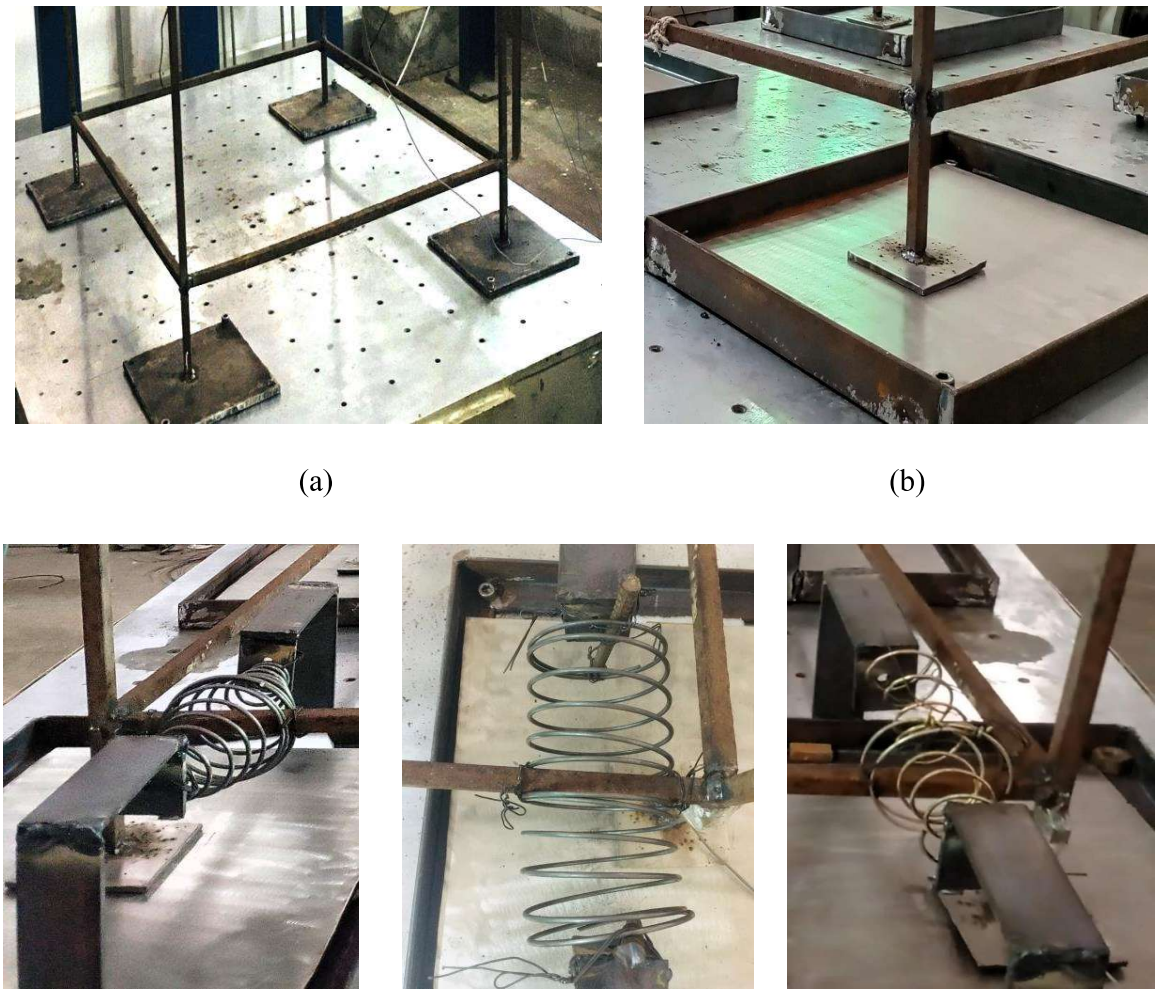

(a) (b)

(c) (d) (e)

Figure 5.18 The different combinations used in this analysis (a) Fixed Base (b) Sliding Base (c) Sliding Base with Conical Spring (d) Sliding Base with Low Stiffness Linear Spring and (e) Sliding Base with High Stiffness Linear Spring

The experimental shaking table results are compared with the numerically simulated results obtained from Abaqus. The comparison revealed a strong correlation, with the Abaqus

simulations accurately replicating the observed experimental behavior. This agreement highlights the reliability and robustness of the numerical model in capturing the dynamic response of the steel frame structures under isolated base combinations.

5.11 Results and Discussion

The results of the shake table tests are presented in the following subsections emphasizing the effect on lateral drift of the model, bearing (slider) displacement, and peak horizontal floor acceleration of the model. From the shake table tests involving the model frame and the five different base conditions (fixed, sliding only and sliding connected with a conical spring, sliding connected with low stiffness linear spring and sliding base connected with high stiffness spring), the responses obtained are discussed.

5.11.1 Inter-story Drift Ratio (IDR)

The experimental results were analyzed in terms of inter-story drift ratio (IDR) and total drift ratio (TDR). The findings revealed that, under fixed-base conditions, a significant amount of force is transmitted to the superstructure during ground excitation. This substantial force transfer can increase the likelihood of damage to both structural and non-structural components attached to the building. Therefore, mitigating this force transfer is critical to safeguarding the integrity of the structural framework and minimizing potential damage to non-structural elements, such as partitions, facades, and equipment, during seismic events. The IDR (%) for frequencies 0.79 Hz, 1.36 Hz, and 1.63 Hz for 25 amplitude is shown in Figure 5.19, Figure 5.20 and Figure 5.21, respectively and for amplitude 45 mm at 0.79 Hz is shown in Figure 5.22. It was observed from the results that increasing the frequency leads to higher IDR (%) and in comparison, to fixed base the other combination shows lower IDR (%) value shows the effectiveness of base isolation.

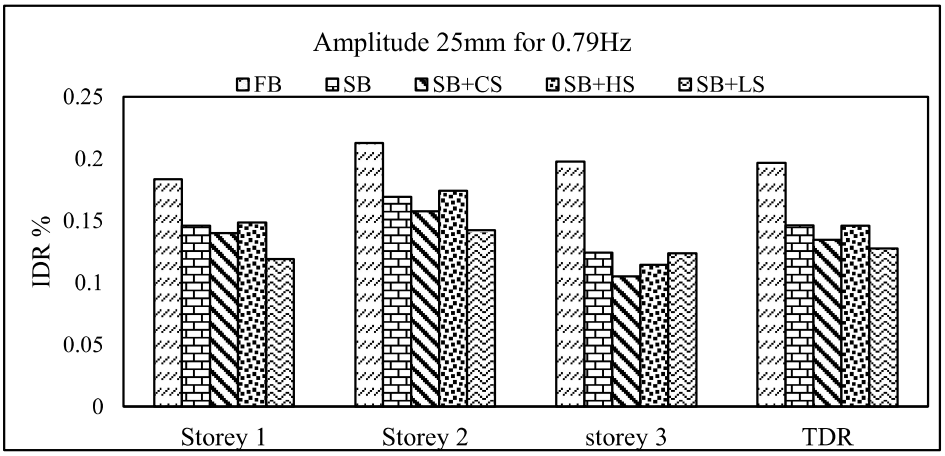

Figure 5.19 IDR (%) at 25mm amplitude for 0.79 Hz frequency.

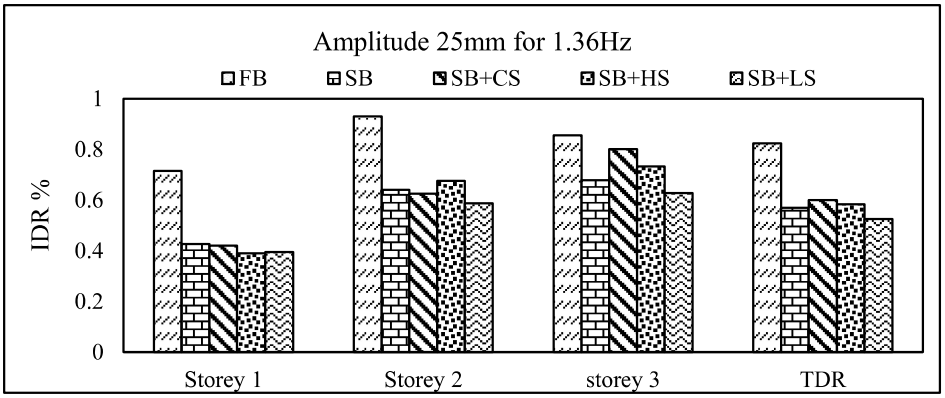

Figure 5.20 IDR (%) at 25mm amplitude for 1.36 Hz frequency.

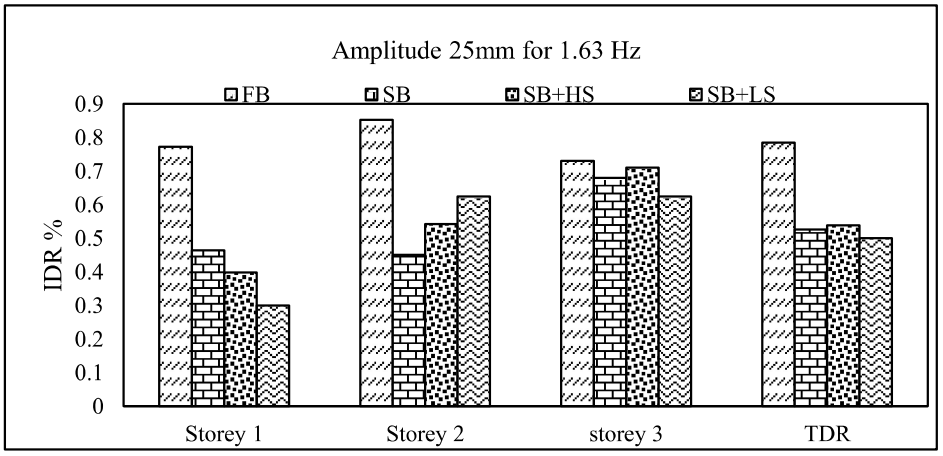

Figure 5.21 IDR (%) at 25mm amplitude for 1.63 Hz frequency.

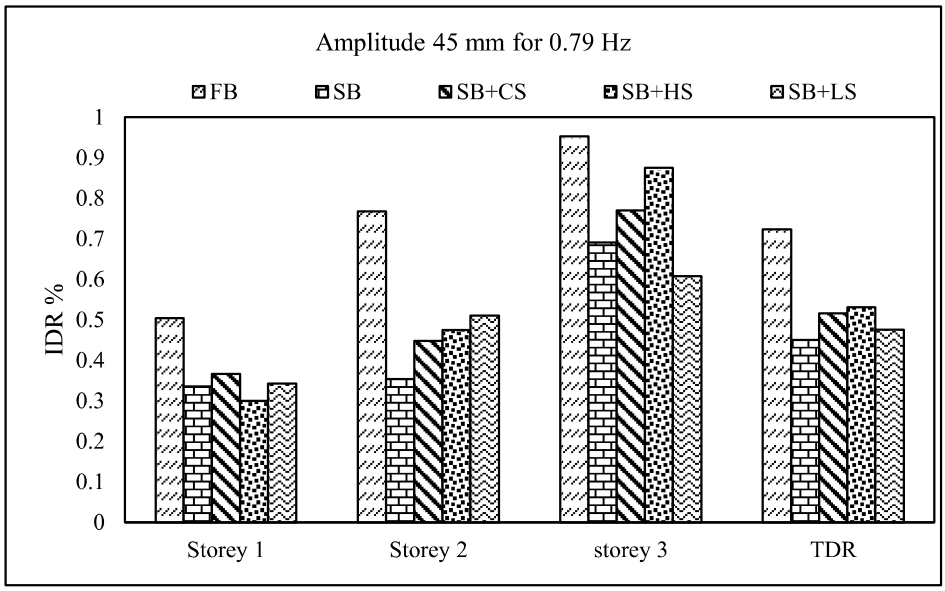

Figure 5.22 IDR (%) at 45mm amplitude for 0.79 Hz frequency.

5.11.2 Peak Top Floor Acceleration

The implementation of sliding isolators, both with and without spring combinations, demonstrates a significant reduction in the acceleration responses at the top floor compared to a fixed-base configuration. This reduction highlights the effectiveness of the proposed model in mitigating seismic forces. The sliding isolator systems efficiently decouple the superstructure from ground motions, thereby limiting the transmission of seismic energy and protecting the structure from excessive accelerations. This performance underscores the potential of such isolation systems in enhancing the seismic resilience of buildings.

The analysis results indicate that the effectiveness of different spring combinations in reducing acceleration responses varies across different frequency ranges.

For an amplitude of **25 mm**, at a **lower frequency of 0.79 Hz**, the reduction in acceleration response is not very significant. However, a maximum reduction of **37.61%** is observed in the

SB configuration, highlighting its effectiveness in mitigating acceleration response at this frequency.

At a **frequency of 0.98 Hz**, the **SB+CS combination** demonstrates the best performance, achieving a **47.32% reduction** in acceleration response. This suggests that the inclusion of a cushioning spring enhances the damping characteristics, leading to improved vibration control.

In the frequency range of **1.24 Hz to 1.36 Hz**, the **SB+LS combination** exhibits significant response reduction. At **1.36 Hz**, this configuration achieves a **34.56% reduction**, indicating its suitability for mitigating vibrations within this frequency range.

At a **higher frequency of 1.63 Hz**, the acceleration response across all combinations becomes negligible, implying that the system reaches a state where vibrations are no longer effectively transmitted. However, in this frequency range, the effect of toppling has been observed, which suggests that stability considerations need to be taken into account when designing such systems.

The **SB+HS combination** achieves a **maximum reduction of 19.83%**, which is relatively lower compared to other configurations. This indicates that while heavy springs contribute to vibration reduction, they may not be as effective as other combinations in higher frequency ranges.

Furthermore, the numerical simulation results closely align with the experimental findings, confirming the observed trends and validating the effectiveness of different spring combinations in reducing acceleration responses across various frequency ranges. The experimental analysis results and percentage reduction are shown in Figure 5.23 and Figure

5.24, respectively, while the numerical analysis results are presented in Figure 5.25 and Figure 5.26 for a 25mm amplitude across different frequencies. Table 5.4 shows the % reduction comparison to fixed base for 25 mm amplitude at 0.98Hz across different frequencies.

Experimental Analysis

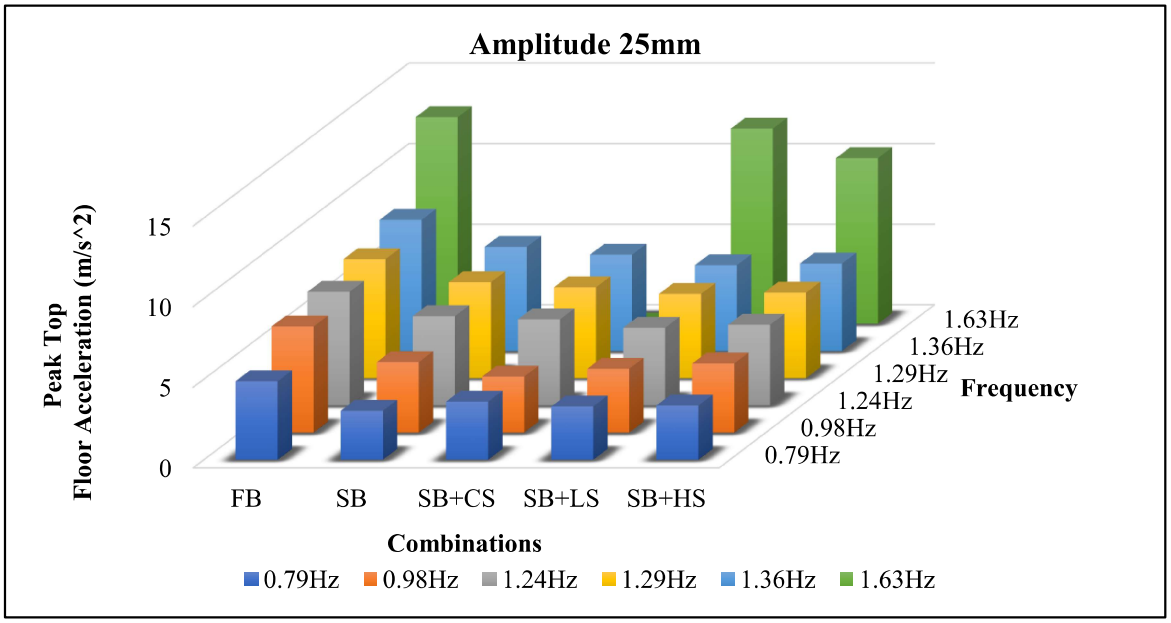

Figure 5.23 Peak top floor acceleration response for 25mm amplitude obtained from experimental analysis

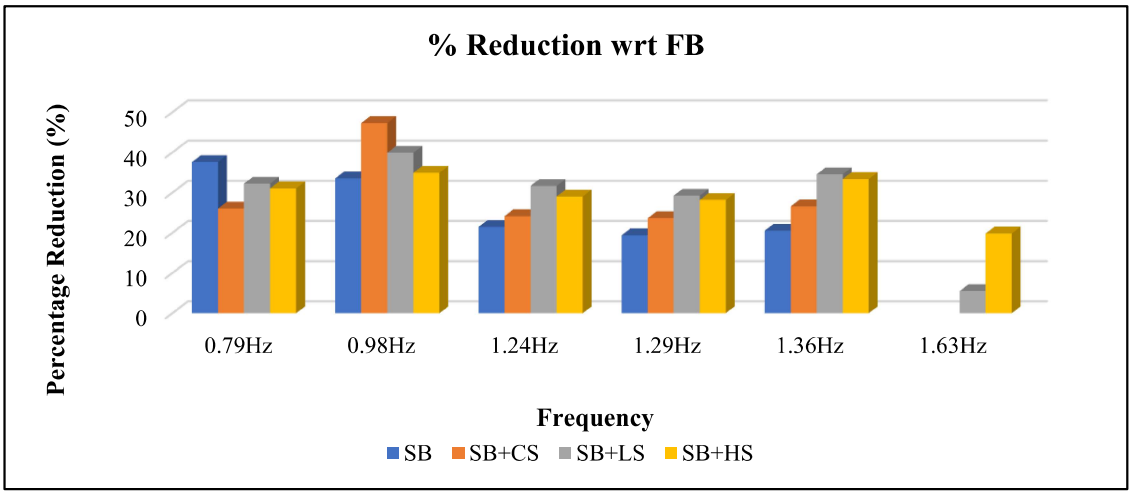

Figure 5.24 Percentage reduction in top-floor acceleration response compared to a fixed base across different frequencies.

Numerical Analysis

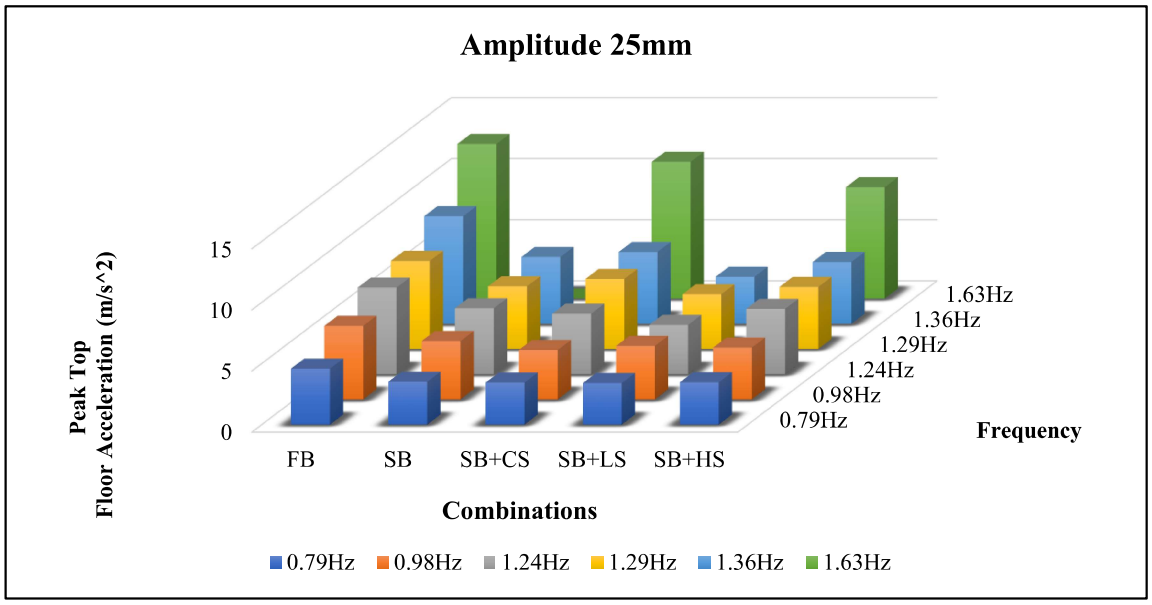

Figure 5.25 Peak top floor acceleration response for 25mm amplitude obtained from numerical abaqus analysis

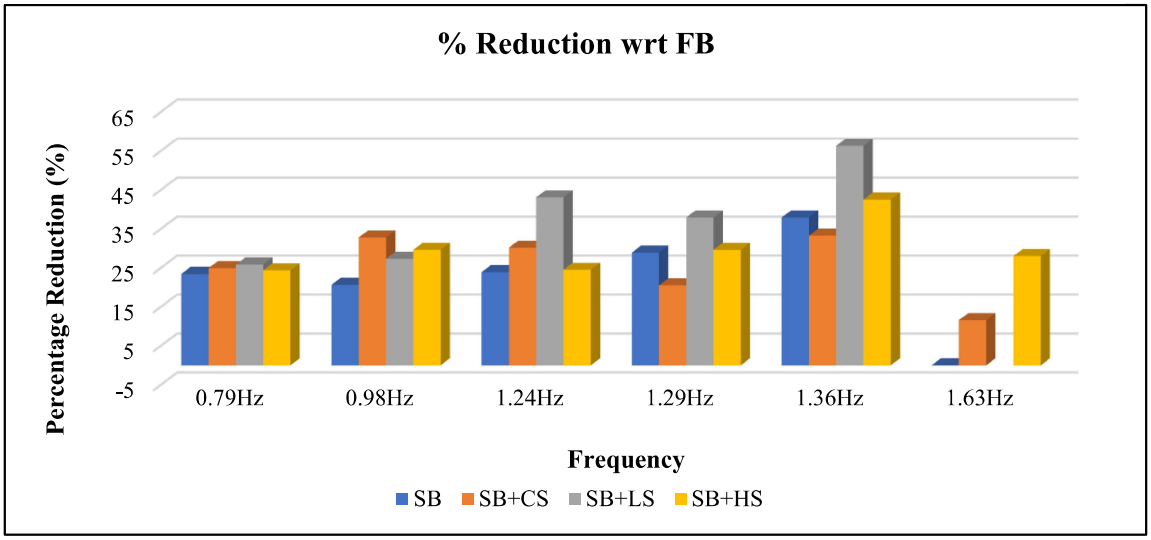

Figure 5.26 Percentage reduction in top-floor acceleration response compared to a fixed base across different frequencies.

Table 5.4 Shows the % reduction for top floor acceleration for all combinations at 0.98Hz for 25 mm amplitude

Isolator Type	% Reduction
Sliding Base	33.55

Sliding Base with conical spring	47.31
Sliding base with high stiffness linear spring	34.93
Sliding base with low stiffness linear spring	39.91

For an amplitude of **45 mm**, the experimental analysis revealed that tests could not be conducted for all frequency combinations beyond **1.24 Hz** due to **instability and toppling** of the system. This indicates that at higher frequencies, the system's stability is significantly affected, making it unsuitable for further experimental evaluation.

At a **low frequency of 0.79 Hz**, the **SB+HS combination** exhibits the **maximum acceleration reduction of 17.17%**, suggesting that incorporating a heavy spring enhances the damping effect in this frequency range.

At **0.98 Hz**, the acceleration response reduction is observed to be **43.58%**, highlighting that the damping characteristics of the system improve as the frequency increases.

At **1.24 Hz**, the **maximum observed acceleration reduction is 50.91%**, demonstrating that the **spring-based isolation system is highly effective in controlling vibrations at this frequency**. However, beyond this frequency, **experimental analysis was not feasible due to toppling effects**, indicating that stability becomes a major concern at higher frequencies for this amplitude.

The **numerical simulation results align well with the experimental observations**, confirming the observed reduction trends and validating the effectiveness of the spring-based isolation system. The experimental analysis results and percentage reduction are shown in Figure 5.27 and Figure 5.28, respectively, while the numerical analysis results are presented in Figure 5.29 and Figure 5.30 for a 45mm amplitude across different frequencies. Table 5.5

shows the % reduction comparison to fixed base for 45 mm amplitude at 0.98Hz across different frequencies.

Experimental Analysis

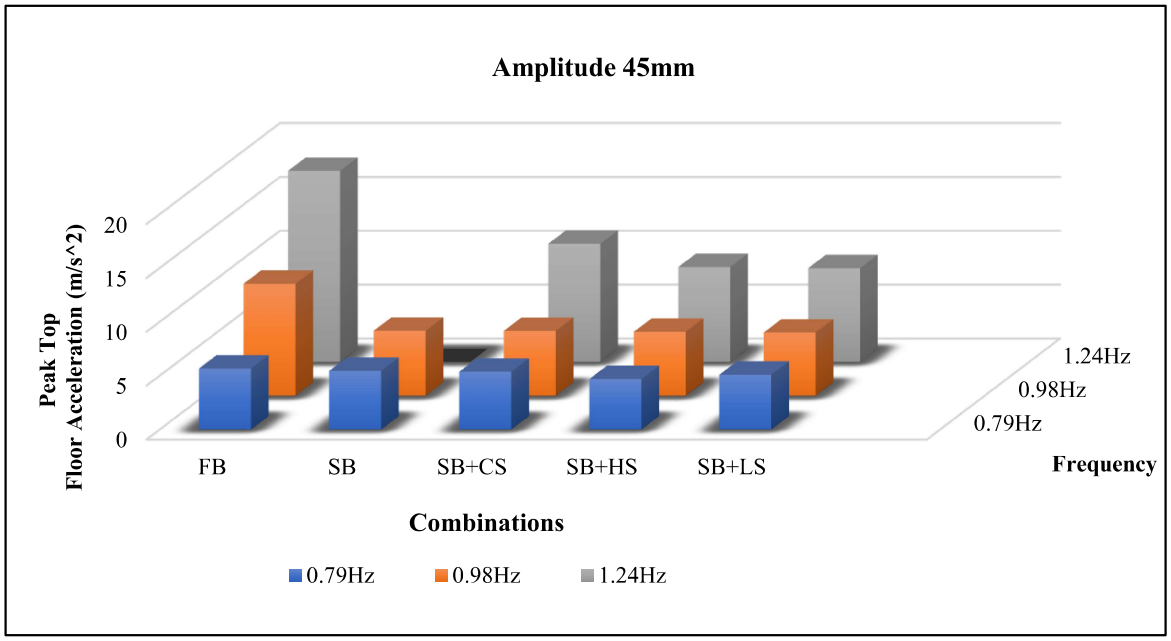

Figure 5.27 Peak top floor acceleration response for 45mm amplitude obtained from experimental analysis

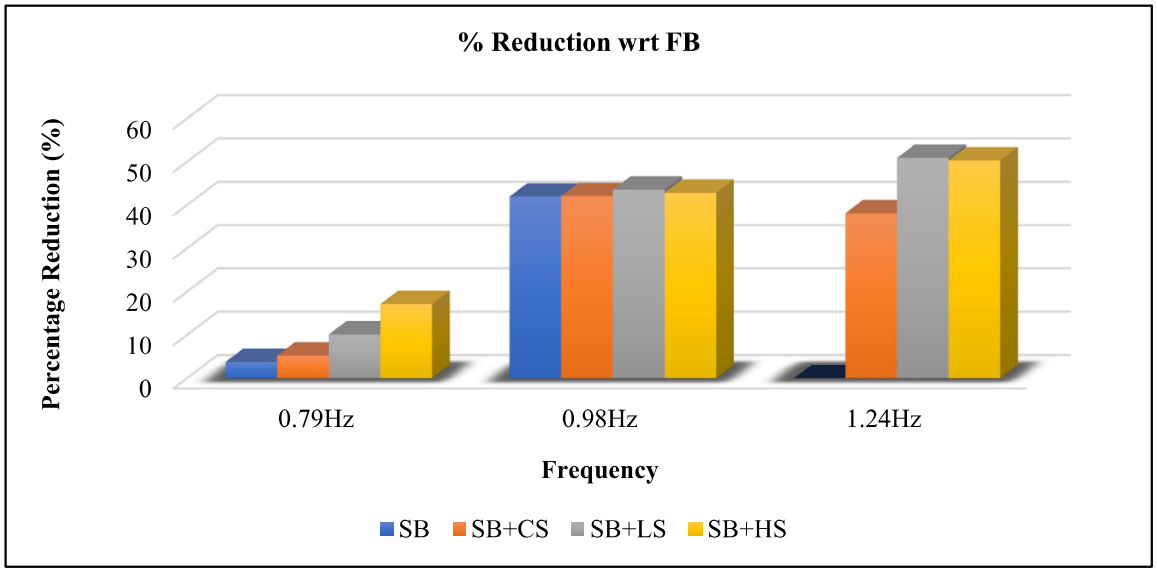

Figure 5.28 Percentage reduction in top-floor acceleration response compared to a fixed base across different frequencies.

Numerical Analysis

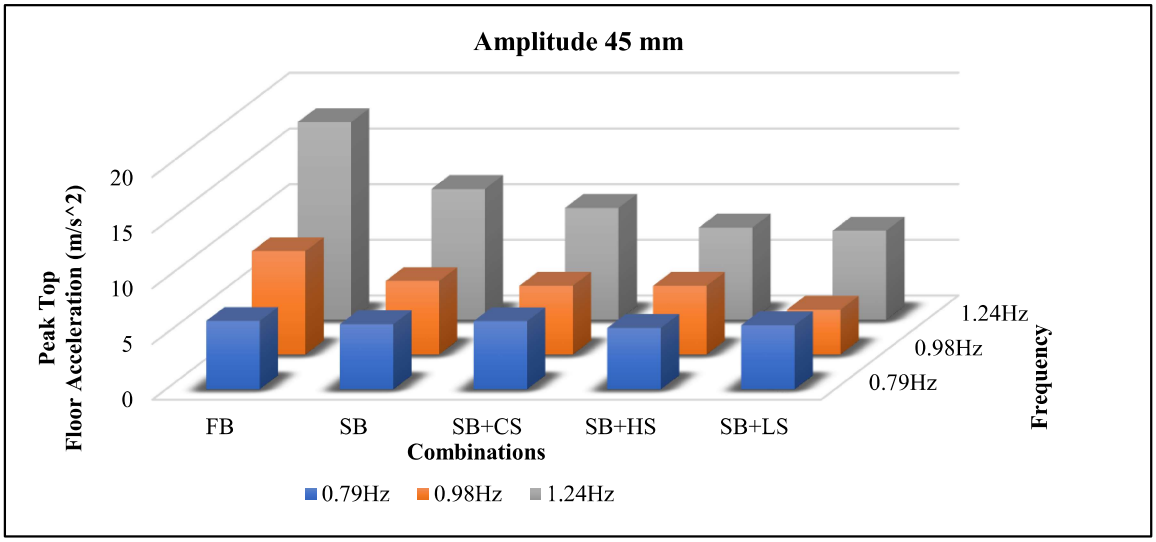

Figure 5.29 Peak top floor acceleration response for 45mm amplitude obtained from numerical abaqus analysis

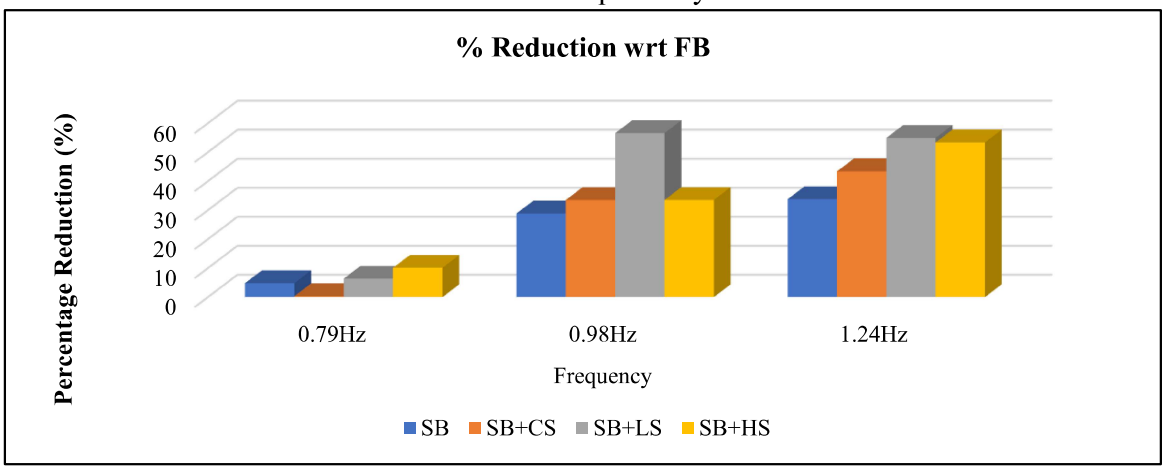

Figure 5.30 Percentage reduction in top-floor acceleration response compared to a fixed base across different frequencies.

Overall, the analysis suggests that **sliding isolation combined with a spring system provides significantly better vibration reduction compared to a sliding base alone** when compared to a fixed base system. This highlights the advantage of incorporating spring elements in sliding isolation systems to enhance seismic performance and mitigate acceleration responses effectively. Although slight variations were observed in some cases between numerical and experimental acceleration results, likely due to experimental limitations, a significant

difference was noted in the percentage variation of top-floor acceleration.

Table 5.5 Shows the % reduction for top floor acceleration for all combinations at 0.98Hz for 45 mm amplitude

Isolator Type	**% Reduction**
Sliding Base	42.0
Sliding Base with conical spring	42.11
Sliding base with high stiffness linear spring	42.87
Sliding base with low stiffness linear spring	43.58

Validation

The experimental and numerical results for the fixed-base condition have been validated across different frequency ranges, showing good agreement with numerical results. The Table 5.6 presents the percentage difference in fixed-base analysis between numerical and experimental results for a 25mm amplitude across different frequencies and Table 5.7 shows the % difference in fixed-base analysis between numerical and experimental results for a 45mm amplitude across different frequencies. Figure 5.31 compares fixed-base numerical and experimental results for top-floor acceleration at a 25mm amplitude, while Figure 5.32 presents the results for a 45mm amplitude.

For 25mm Amplitude

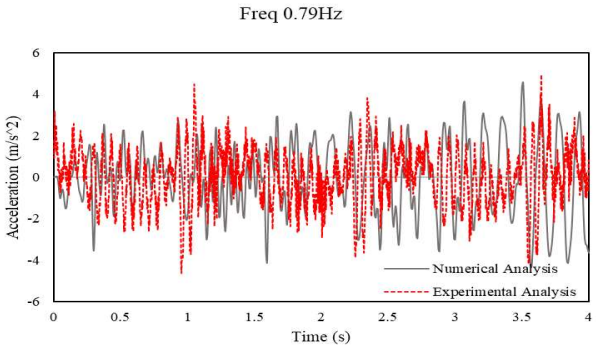

(a)

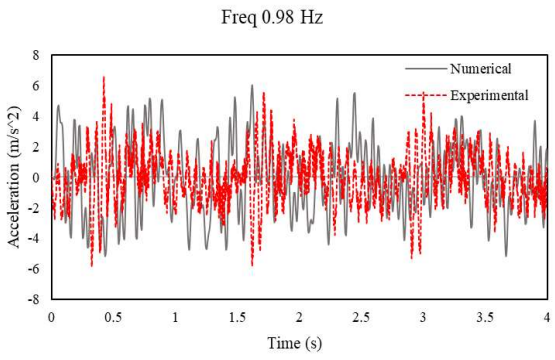

(b)

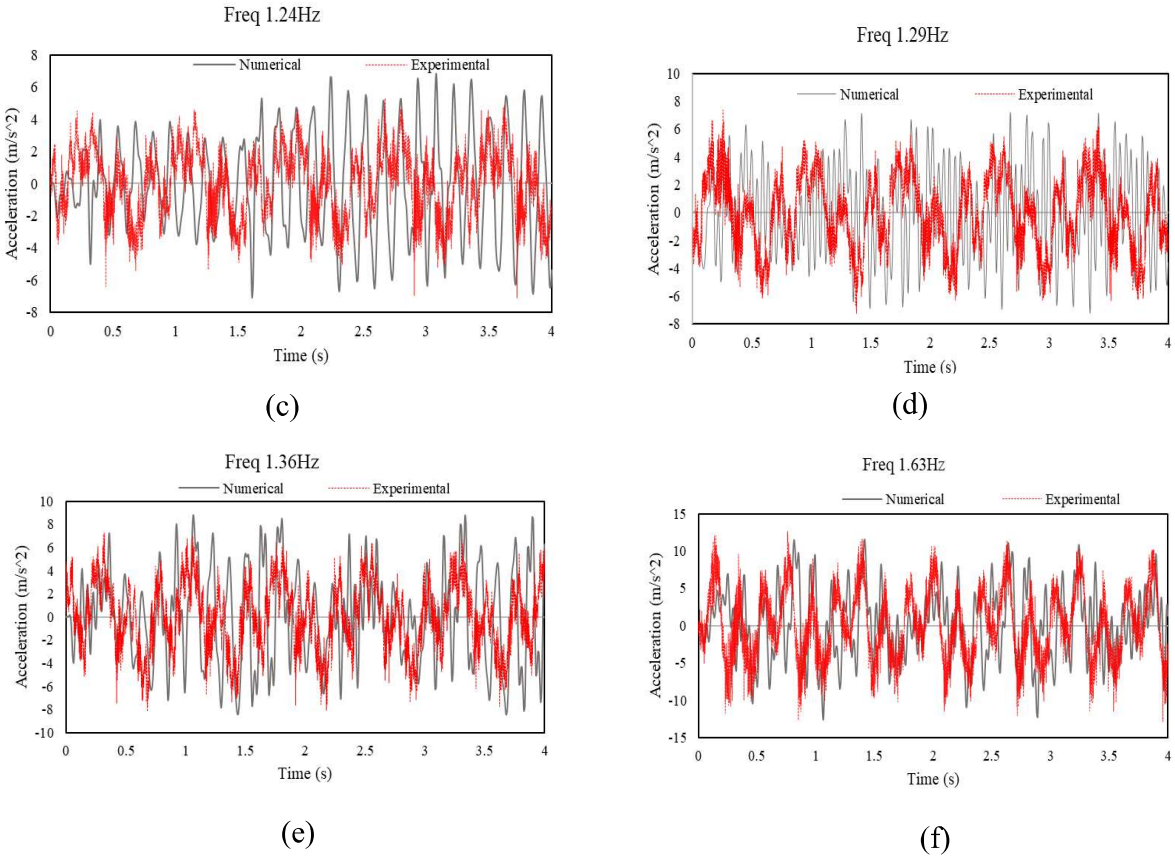

Figure 5.31 Comparison of numerical and experimental fixed-base results across different frequency ranges for 25mm amplitude.

Table 5.6 Shows the % difference in fixed base analysis in numerical and experimental analysis for 25mm amplitude across different frequencies.

Input Frequency	**Experimental Analysis (m/s^2)**	**Numerical Analysis (m/s^2)**	**% Difference**
0.79 Hz	4.87	4.57	6.08
0.98 Hz	6.5	6.01	8.58
1.24 Hz	7.04	7.07	0.53
1.29 Hz	7.38	7.20	2.46
1.36 Hz	8.13	8.79	`8.12
1.63 Hz	12.81	12.6	1.28

For 45 mm Amplitude

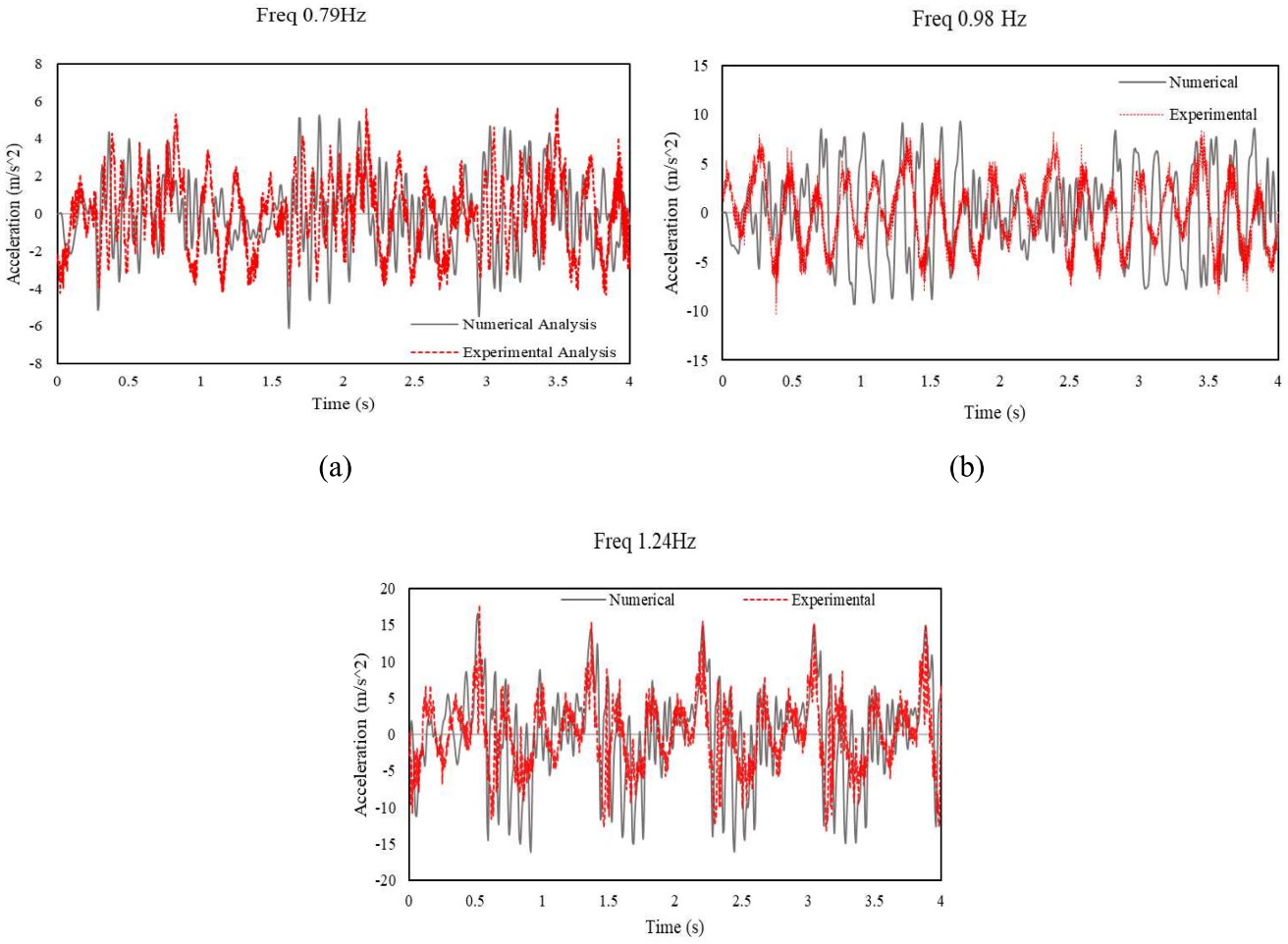

Figure 5.32 Comparison of numerical and experimental fixed-base results across different frequency ranges for 45mm amplitude.

Table 5.7 Shows the % difference in fixed-base analysis between numerical and experimental results for a 45mm amplitude across different frequencies.

Input Frequency	Experimental Analysis (m/s^2)	Numerical Analysis (m/s^2)	% Difference
0.79 Hz	5.65	6.13	8.45
0.98 Hz	10.38	9.28	10.65
1.24 Hz	17.75	16.49	7.10

The following limitations have been considered in this study:

1. The friction coefficient has been assumed to remain constant throughout the experimental process on the shaking table test, with a value of 0.23.
2. It is assumed that the model behaves similarly without torsion and deformation throughout the experimental process, regardless of the input frequency.
3. Material properties such as damping and stiffness are considered to remain linear and unchanged during the tests, without accounting for potential nonlinearity or degradation over time.
4. The influence of multi-directional or combined input motions has not been considered, as the study focuses solely on uni-directional input frequencies.
5. Variations in environmental conditions, such as temperature or humidity, which may affect material behavior, have been ignored.

5.12 Summary

The present chapter deals with the acceleration and IDR response of the of the three-story moment resisting steel frame structure inserted with sliding bearing attached with and without spring combination. A numerical model, developed based on the experimental setup and friction data, effectively replicates the experimental observations. Specifically, for a given ground motion, the numerical model accurately captures the peak top floor acceleration observed during the experiments. It was observed that an increase in the amplitude of ground motion leads to a corresponding rise in the structural responses. Additionally, the inter-story drift ratio increases as the applied responses, characterized by the frequency input in the shake table tests, are intensified.